

Electronic Supplementary Information

Electrochemical performance of a Li⁺-enriched metallohydrogel as electrolyte and electrode materials for supercapacitors

Yeeshu Kumar,^a Moupia Mukherjee,^a Manish Kumar Dixit,^a Abul Kalam^b and Mrigendra Dubey*^a

^aSoft Materials Research Laboratory, Department of Metallurgical Engineering and Materials Science, Indian Institute of Technology Indore, Indore 453552, India.

Email: mdubey@iiti.ac.in

^bDepartment of Chemistry, College of Science, King Khalid University, Abha 61413, Saudi Arabia.

<u>Table of Contents:</u>	<u>Pages</u>
EXPERIMENTAL SECTION	
Material and physical methods	S2
Rheological Study	S2
Transport Number Evaluation	S3
Electrochemical Characterization	S3
Synthesis and Characterization	S4
Scheme S1	S4
Supplementary Figures	
Figure S1	S5
Figure S2	S5
Figure S3	S6
Figure S4	S6
Figure S5	S7
Figure S6	S7
Figure S7	S8
Figure S8	S8
Figure S9	S9
Figure S10	S9
Figure S11	S9
Figure S12	S10
Table S1	S10
Table S2	S11

EXPERIMENTAL SECTION

Materials and Physical Methods:

Common reagents and solvents used in the current work were procured from Advent chembio Pvt. Ltd, Navi Mumbai India and Finar Ltd, Ahmedabad, India. Lithium hydroxide and 5-aminosalicylic acid were purchased from Spectrochem Pvt. Ltd., Mumbai (India). Cobalt(II) acetate tetrahydrate was procured from Sisco Research Laboratories Pvt. Ltd. Mumbai (India). Hexamethylene tetramine, trifluoroacetic acid, Phloroglucinol were purchased from Sigma-Aldrich.

Fourier transform infrared (FT-IR) spectra were recorded by using spectrum two FT-IR spectrometer (PerkinElmer). PerkinElmer's Lambda 365 spectrophotometer was used to carry out UV-Vis absorption study. ^1H and ^{13}C NMR spectra was recorded on a AVNACE NEO500 Ascend Bruker BioSpin International AG, Switzerland. Electrospray ionization mass spectra were obtained by using LC-MS Q-ToF. Field emission scanning electron microscopic (FESEM) images were obtained using a JOEL-7610F Plus microscope. Powder X-ray diffraction (PXRD) data were collected within the 2θ range of 10 to 70° using an Empyrean instrument from Malvern Panalytical. Thermal gravimetric analysis (TGA) experiments were conducted on a STA 8000 thermal analyzer from PerkinElmer, ramping the temperature from 30 to 700°C at a rate of 10°C per minute.

Rheological Study:

As synthesized metallohydrogels (1% w/v) samples were subjected to rheological experiments with the help of an Anton Paar's rotary rheometer MCR 102. The samples were placed in between two stainless steel parallel plates with diameter 20 mm and maintaining 1.0 mm gap. Dynamic amplitude sweep measurements were carried out to the linear viscoelastic regions (LVR) of the metallohydrogels (**MG-Co**) by recording the storage and loss moduli (G' , G'') against applied stress and strain, respectively at constant frequency of 10 rad/sec. Dynamic oscillatory frequency sweep measurements were conducted at room temperature (25°C) within the range of 0.1 to 100 rad/sec at a constant shear strain of 1%.

Transport number evaluation

Lithium-ion transport number (t_{Li^+}) were determined for freshly synthesized metallohydrogels (**MG-Co**) through the utilization of d.c. polarization and electrochemical impedance spectroscopic methods. In this process, a voltage step of 0.75 volts was applied to the electrochemical cell setup, denoted as SS|**MG-Co**|SS, to induce polarization. The resulting current output was recorded over time, as depicted in Figure 9. The calculation of lithium-ion transport number (t_{Li^+}) was carried out using a standard equation:

$$t_{\text{Li}^+} = \frac{I_s(\Delta V - I_0 R_0)}{I_0(\Delta V - I_s R_s)} \dots \dots \dots (2)$$

Where, I_0 and I_s represent the initial current and steady-state current, respectively, both obtained from the dc polarization measurements. R_0 signifies the cell resistance before the polarization experiment, while R_s represents the cell resistance after the polarization experiment. It's worth noting that the values of R_0 and R_s

were extracted from Nyquist plot measurements. Lastly, ΔV denotes the applied step voltage.

Electrochemical Characterization:

The working electrodes were prepared using the **MG-Co** xerogel as active materials which was mixed with activated carbon and polyvinylidene fluoride (PVDF) in a mass ratio 75:20:5. Further, obtained mixture was dispersed in N-Methyl-2-Pyrrolidone (NMP). The resulting slurry was spread onto the nickel foam (12 mm diameter) and then dried under vacuum at 70 °C for 8 h. Further, the coated nickel foam was pressed using palletizer. Moreover, **MG-Co-Li** gel and 1M LiOH were used as electrolyte in the three-electrode system. The mass of the active material was in the range of 1.5–2.5 mg. All the electrochemical measurements were carried out on a CHI 608E electrochemical workstation (CH Instruments) with a three-electrode configuration, where Pt wire was used as the counter electrode and an Ag/AgCl as the reference electrode under normal atmospheric conditions. Cyclic voltammetry (CV) was carried out from –0.6 to 0.6 V potential window at various scan rates of 10–100 mV/s. Galvanostatic charge–discharge (GCD) curves were conducted in the potential range of –0.85 to 0.5 V at different constant current density. Electrochemical impedance spectroscopic (EIS) measurements were carried out in a frequency range of 0.1 Hz to 1 MHz at open-circuit potential with an ac perturbation of 10 mV.

Synthesis and characterization:

Synthesis of 2,4,6-trihydroxybenzene-1,3,5-tricarbaldehyde

10 g (71.5 mmoles) of Hexamethylene tetramine (HMTA) were dissolved in 40 ml of trifluoroacetic acid (TFA) and slowly added drop by drop to a suspension of phloroglucinol (3.98 g or 31.5 mmoles) in TFA (20 mL). The resulting mixture was then subjected to reflux for a period of 5 hours. Subsequently, 150 mL of 3M hydrochloric acid (HCl) were introduced into the resulting orange solution, and the mixture was kept under reflux for an additional 2 hours. The resultant solution was extracted three times using 150 mL of dichloromethane (DCM) and then dried using anhydrous magnesium sulfate ($MgSO_4$). After filtration, the solution was vacuum-dried to yield a fine powder with a yellowish-orange colour. Yield 1.4 g (16%). 1H NMR (d_6 -DMSO, 400 MHz, δ_H , ppm) 14.04 (s, 3H, -OH), 10.08 (s, 3H, -CHO).

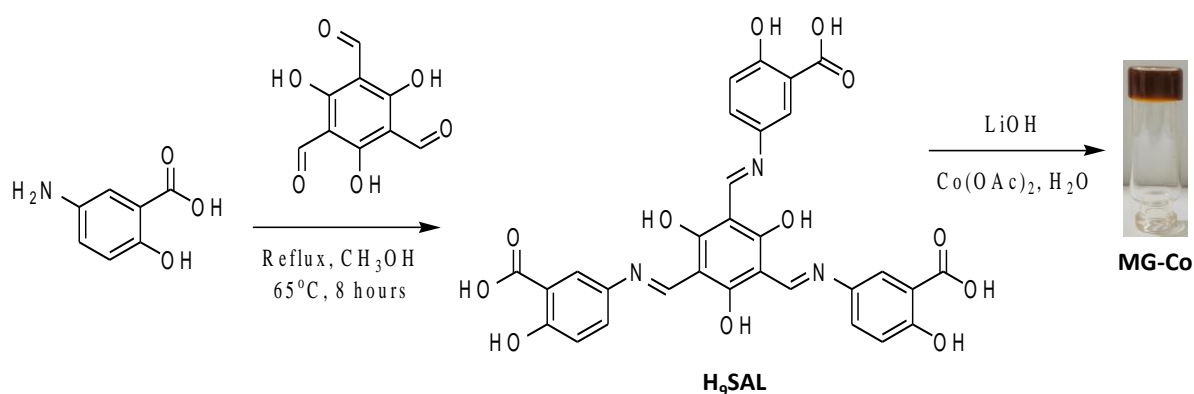
Synthesis of H_9SAL gelator molecule

2,4,6-trihydroxybenzene-1,3,5-tricarbaldehyde (0.1 g, 0.475 mmol) dissolved in methanol was added dropwise to a methanolic solution of 5-aminosalicylic acid (0.218 g, 1.423 mmol) and the obtained suspension was kept on reflux for 8 hours at 65 °C. It afforded brown colored solid compound, this compound was filtered, washed with methanol, diethyl ether followed by vacuum drying. Yield 0.270 g (80%). Anal. calcd. for $C_{30}H_{21}N_3O_{12}$: C, 58.54; H, 3.44; N, 6.83; Found: C, 58.33; H, 3.20; N, 6.63. 1H NMR (d_6 -DMSO, 500 MHz, δ_H , ppm) 6.83 (s, 3H, Ar-H), 7.37 (s, 3H, Ar-H), 7.80 (s, 3H, Ar-H), 8.65 (s, 3H, -HC=N). ^{13}C NMR (d_6 -DMSO, 500 MHz, δ , ppm) 105.28, 119.32, 123.67, 129.58, 149.76, 162.32, 173.40, 184.75, 207.12. FT-IR (ATR, cm^{-1}): $\nu(-OH)$ 2876, 3043, $\nu(-C=O)$ 1607, 1673. ESI-MS m/z : [$C_{30}H_{13}N_3O_{12}.Li_8.H_2O$] $^+$, 681.16 (*calcd.* 681.18). The H_9SAL was deprotonated with LiOH for NMR characterization due to insolubility of H_9SAL in DMSO solvent.

Synthesis of MG-Co metallohydrogel

H_9SAL (20 mg, 0.032 mmol) was first dissolved in 0.5 mL of deionized water in a vial. Subsequently, it was deprotonated using LiOH.H₂O (12.28 mg, 0.28 mmol) and then subjected to sonication. This process

led to the formation of a dark red transparent solution. To this solution, a freshly prepared solution of $\text{Co}(\text{OAc})_2 \cdot 4\text{H}_2\text{O}$ (13 mg, 0.048 mmol) in 0.5 mL of deionized water was added drop by drop. Over time, the solution gradually transformed into a dark red-colored gel, which we refer to as **MG-Co**. To confirm the formation of the gel, we employed the inverted vial test method. Anal. calcd. for $\text{C}_{30}\text{H}_{13}\text{N}_3\text{O}_{12}\text{Co}_2\text{Li}_3 \cdot (\text{H}_2\text{O})_6$: C, 39.43; H, 2.75; N, 4.60; Found: C, 39.38; H, 2.68; N, 4.56. FT-IR (ATR, cm^{-1}): $\nu(-\text{OH})$ 3290, $\nu(-\text{C}=\text{O})$ 1555, 1611. ESI-MS (diluted gel) m/z : $[\text{C}_{30}\text{H}_{17}\text{N}_3\text{O}_{12}\text{Co} \cdot \text{H}_2\text{O} \cdot \text{Li}_2 + \text{H}]^+$, 703.05 (*calcd.* 703.06), $[(\text{C}_{30}\text{H}_{13}\text{N}_3\text{O}_{12})\text{Co}_2 \cdot \text{H}_2\text{O} \cdot \text{Li}_2 + \text{H}]^+$, 771.91 (*calcd.* 771.99) and $[(\text{C}_{30}\text{H}_{13}\text{N}_3\text{O}_{12})\text{Co}_3 \cdot (\text{H}_2\text{O})_6 \cdot \text{Li}_2 + \text{H}]^+$, 906.94 (*calcd.* 906.95).



Scheme S1: Synthetic route adapted for the synthesis of **H₉SAL** and **MG-Co**.

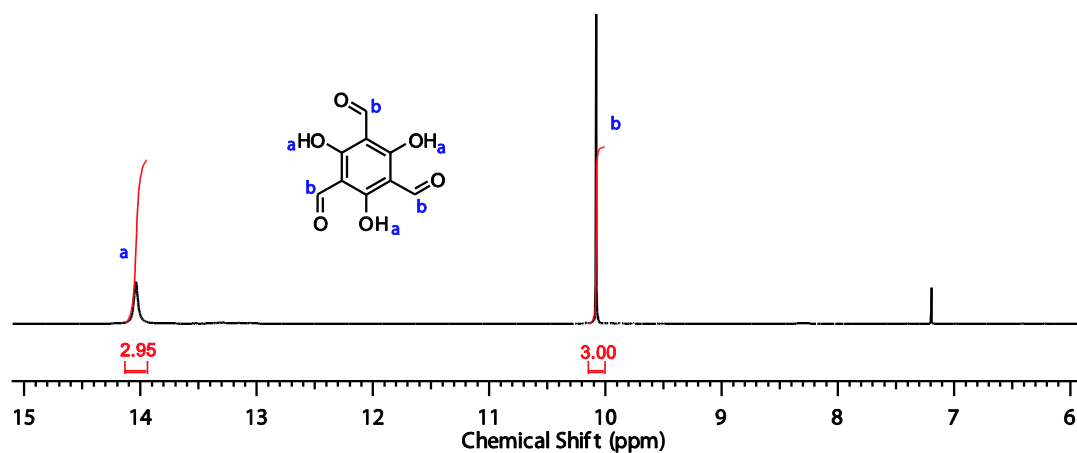


Figure S1. ^1H NMR spectrum of 2,4,6-trihydroxybenzene-1,3,5-tricarbaldehyde.

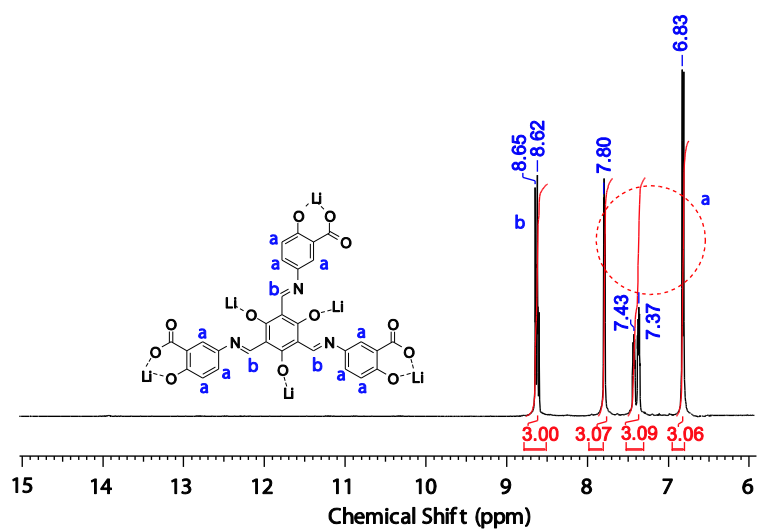


Figure S2. ^1H NMR spectrum of LiOH deprotonated H_9SAL ($\text{DMSO-}d_6$, 500 MHz)

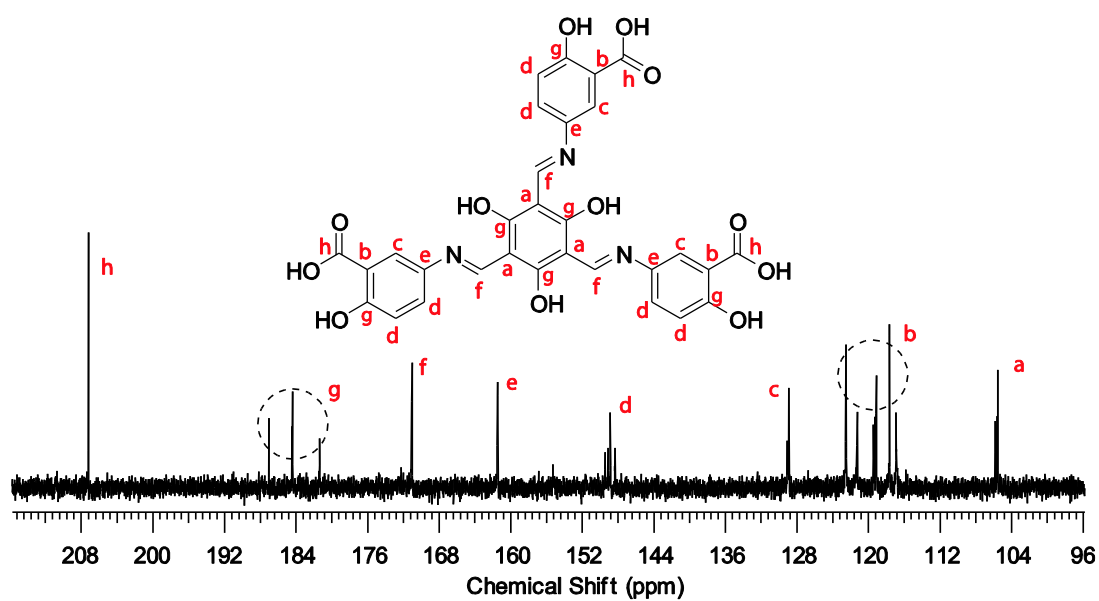


Figure S3. ^{13}C NMR spectrum of LiOH deprotonated H_9SAL ($\text{DMSO-}d_6$, 500 MHz).

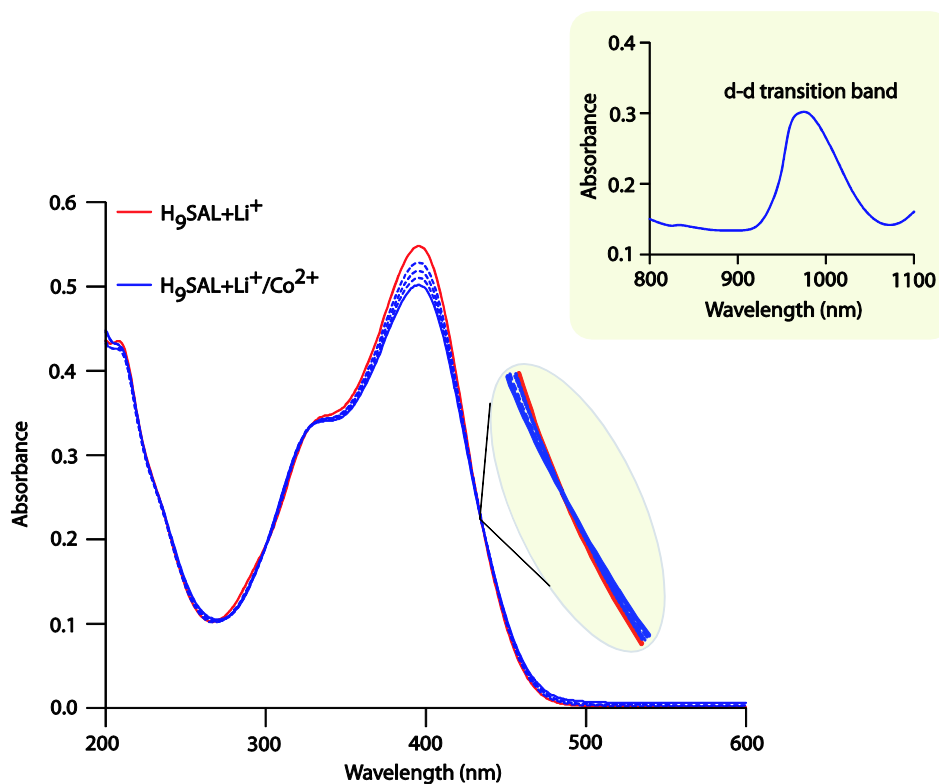


Figure S4. (A) UV-vis titration spectra of $\text{H}_9\text{SAL}+\text{Li}^+$ (1×10^{-5} M, H_2O , red line) vs Co^{2+} (1×10^{-3} M, H_2O , blue lines).

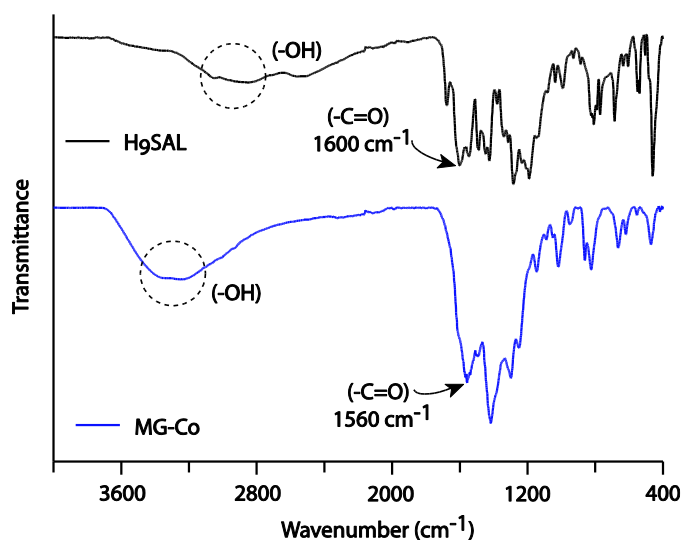


Figure S5. FT-IR spectrum of H_9SAL gelator (black) shows $\nu(\text{-OH})$ at 2876, 3043 cm^{-1} , $\nu(\text{-C=O})$ at 1600, 1680 cm^{-1} . FT-IR spectrum of MG-Co xerogel (blue) shows $\nu(\text{-OH})$ at 3290 cm^{-1} , $\nu(\text{-C=O})$ at 1555, 1611 cm^{-1}

Note: Binding of Co^{2+} to the the -COOH and -OH chelating sites of H_9SAL causes appreciable shift in vibrational bands corresponding to the -C=O and -OH bonds.

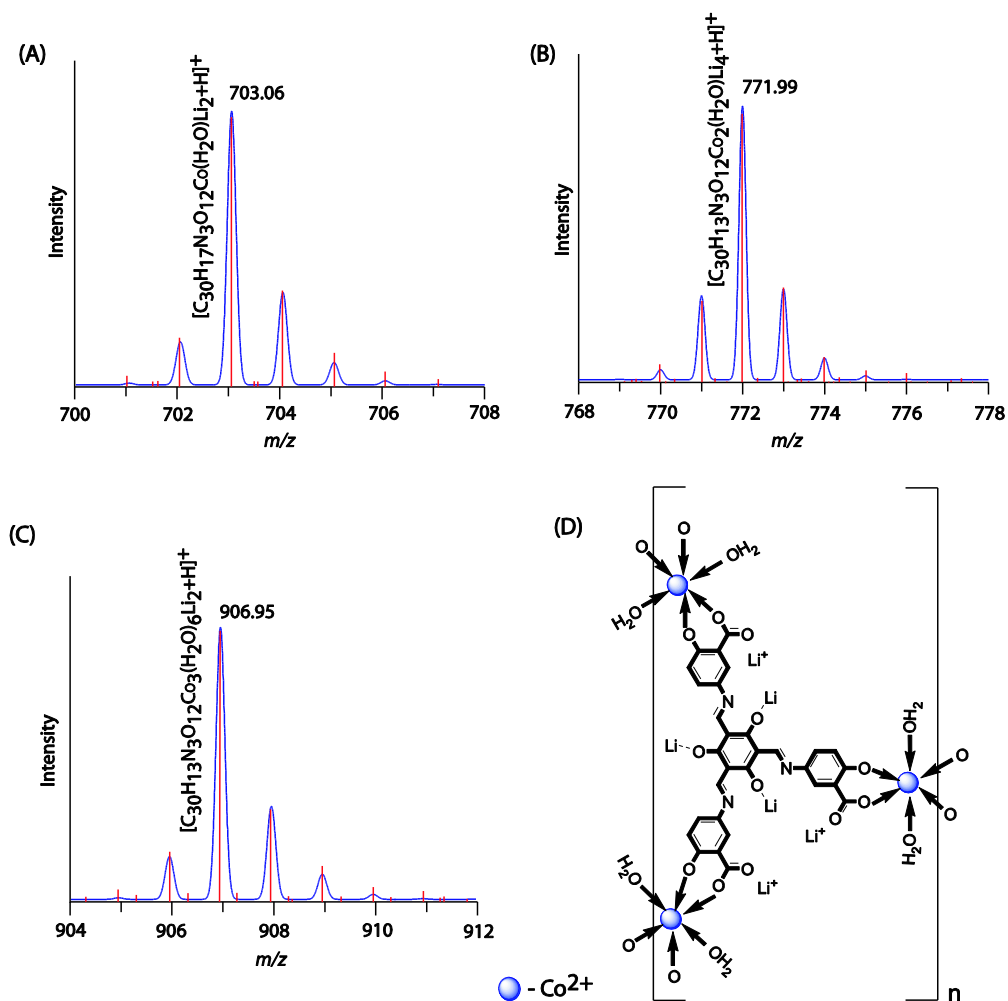


Figure S6. (A-C) ESI-MS spectra of diluted **MG-Co**: Isotopic abundance patterns corresponding to the molecular ion species $[C_{30}H_{17}N_3O_{12}Co \cdot (H_2O) \cdot Li_2 + H]^+$, $[C_{30}H_{13}N_3O_{12}Co_2 \cdot (H_2O) \cdot Li_4 + H]^+$ and $[C_{30}H_{13}N_3O_{12}Co_3 \cdot (H_2O)_6 \cdot Li_2 + H]^+$; (D) Chemical structure of the **MG-Co** confirmed with help of various instrumental techniques.

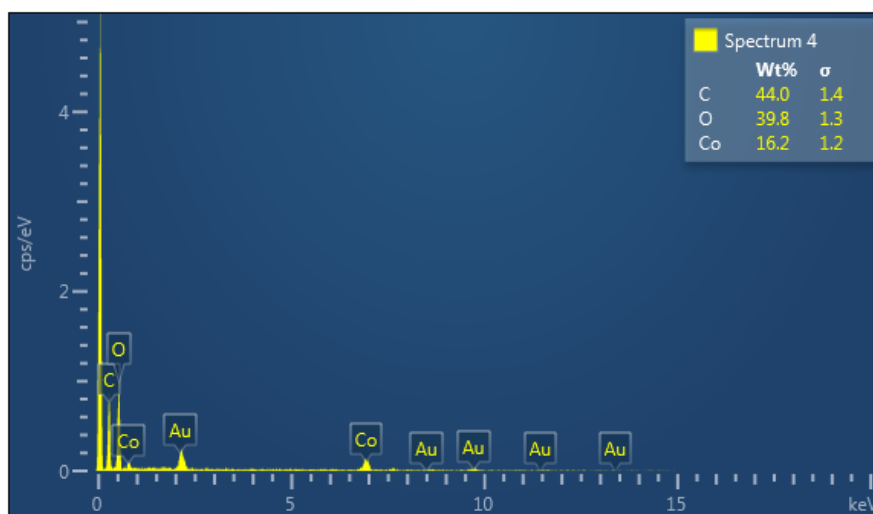


Figure S7. (A) EDS spectrum of **MG-Co** xerogel showing presence of C, O and Co elements. Note: The EDS analysis provided the average weight percentage of Co element to be ~ 12.47%.

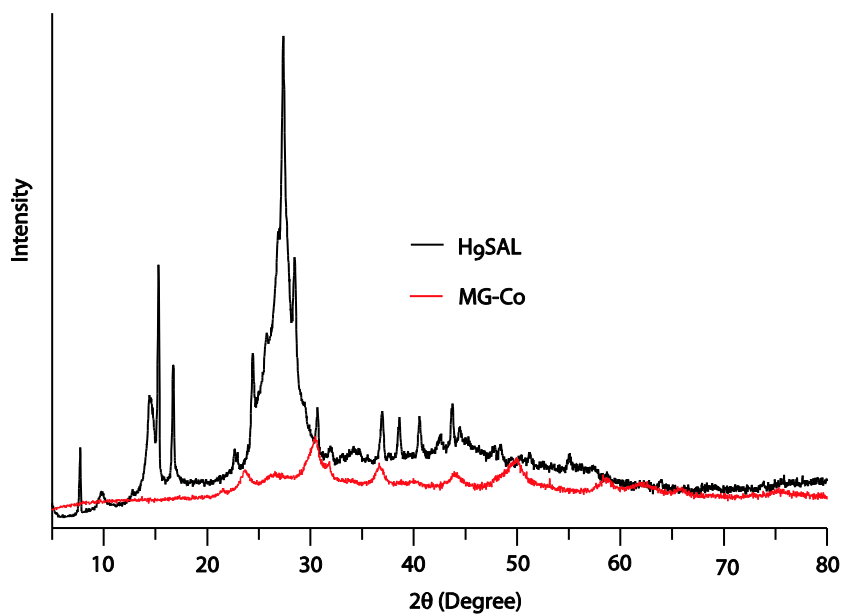


Figure S8. Powder XRD patterns of **H₉SAL** and **MG-Co** xerogel.

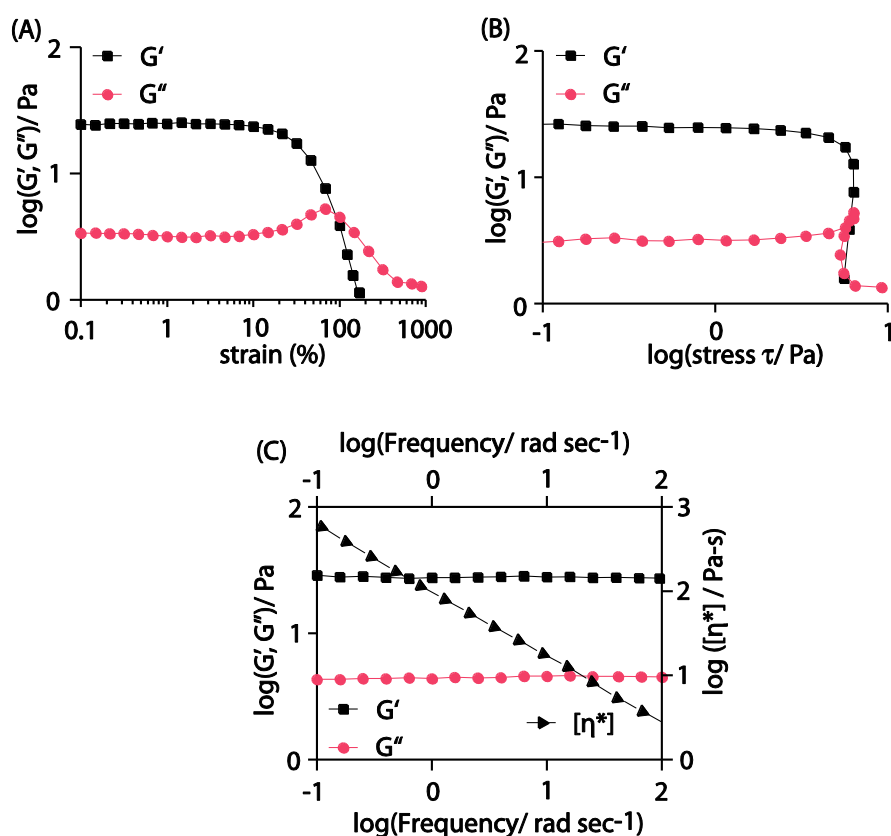


Figure S9. Rheological study over freshly prepared **MG-Co** metallohydrogel (A) Variation in G' and G'' at a frequency of 10 rad s^{-1} and $25 \text{ }^\circ\text{C}$ under strain sweep, (B) Variation in G' and G'' at a frequency of 10 rad s^{-1} and $25 \text{ }^\circ\text{C}$ under stress sweep, (C) Variation of G'' and G' against oscillatory frequency.

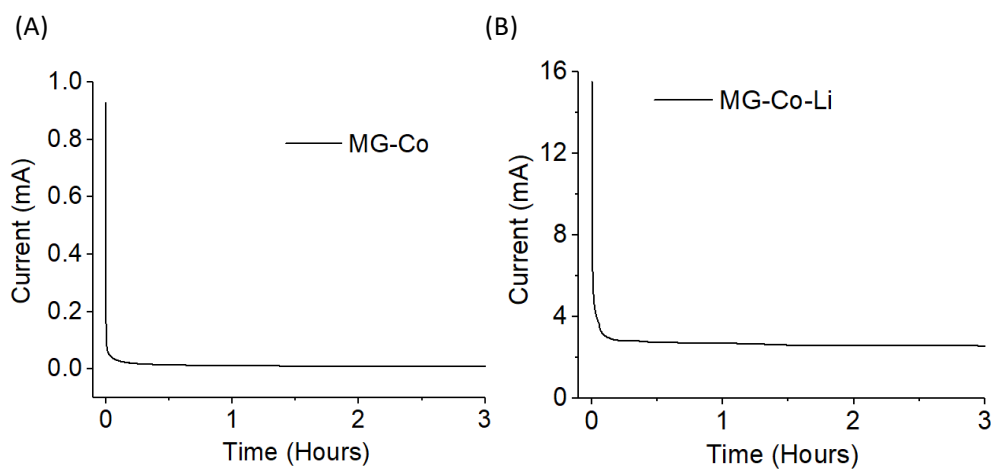


Figure S10. D.C. polarization curve of cell: (A) SS|MG-Co|SS and (B) SS|MG-Co-Li|SS, at applied step potential of 0.75 V.

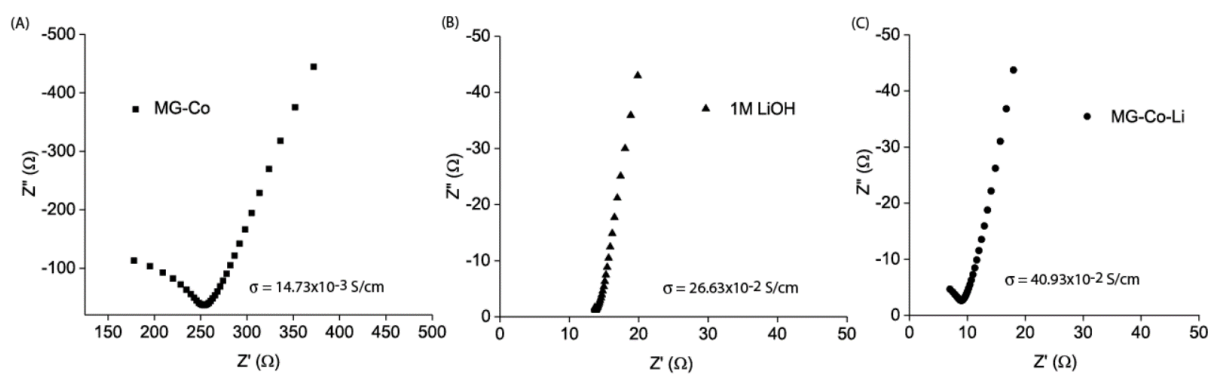


Figure S11. Nyquist impedance plots (A) MG-Co, (B) 1M LiOH aqueous solution, (C) MG-Co-Li.

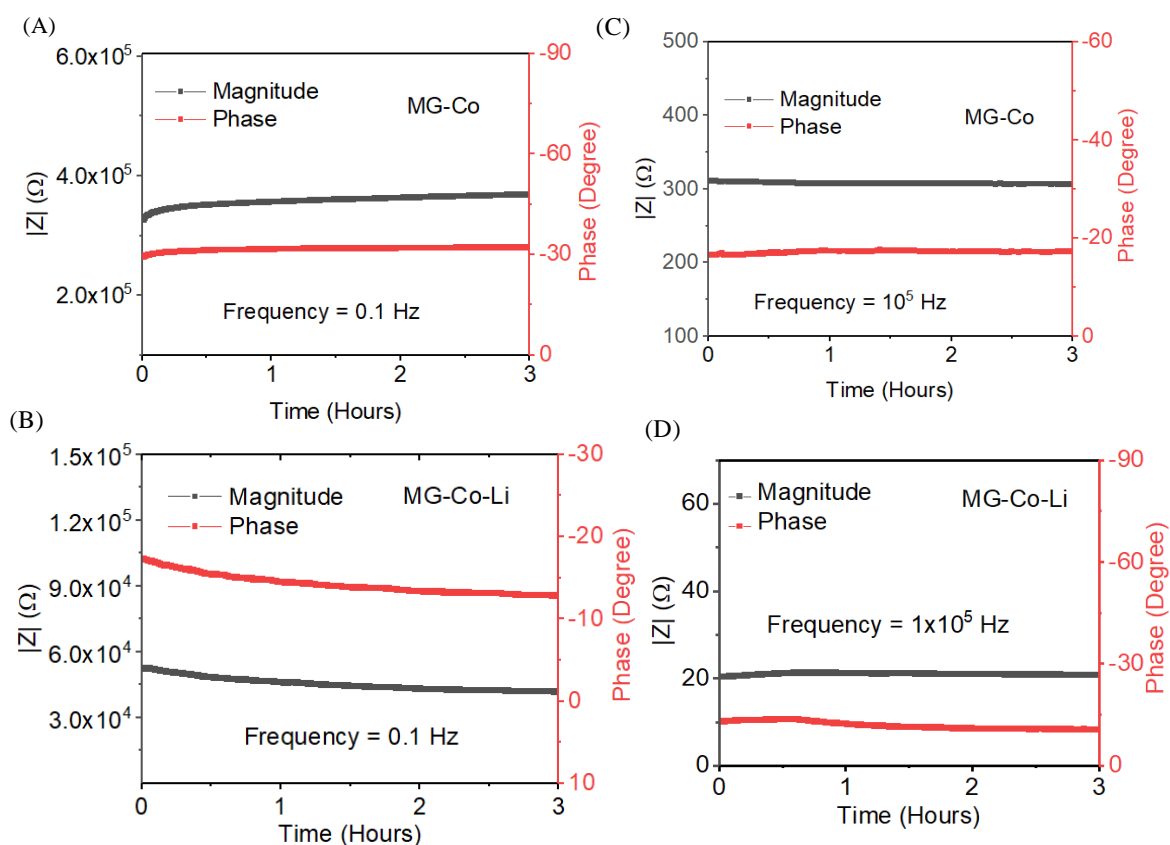


Figure S12. (A and B) Impedance variation with time at 0.1 Hz for **MG-Co** and **MG-Co-Li** respectively, (C and D) Impedance variation with time at 10^5 Hz for **MG-Co** and **MG-Co-Li** respectively.

Table S1. Specific capacitance measured for MG-Co xerogel electrode with 1M LiOH aqueous electrolyte and MG-Co-Li gel electrolyte at various current densities.

Current densities (A/g)	Specific capacitance (F/g)	
	MG-Co xerogel electrode with 1M LiOH aqueous electrolyte	MG-Co xerogel electrode with MG-Co-Li gel electrolyte
1	65.5	86.0
1.5	40.8	49.2
2	23.4	25.6
2.5	14.3	16.2

Table S2. Comparison of electrochemical data reported in the current work with previously reported research work.

Electrolyte	Electrode Material	Function	Specific capacitance (F/g)	Current density (A/g)	References
Zinc containing metal-organic gel	Activated carbon	Only as electrolyte	47.26	1	C. K. Karan <i>et al.</i> , <i>Chem. Eur. J.</i> , 2019, 25 , 14775.
1M KOH	Sb-COF	Only as electrode material	78.6	3	K. Kang <i>et al.</i> , <i>Chem. Commun.</i> , 2022, 58 , 3649.
6M KOH	DBT-MA-COF	Only as electrode material	90	1	L. Li <i>et al.</i> , <i>Microporous Mesoporous Mater.</i> , 2021, 312 , 110766.
H ₂ SO ₄ /PVA gel	Hex-Aza-COF-3	Only as electrode material	64	1	S. Kandambeth <i>et al.</i> , <i>Adv. Energy Mater.</i> , 2020, 10 , 2001673.
1 M Na ₂ SO ₄	[C60]0.05-COF	Only as electrode material	47.6	1	X. Zhao, <i>et al.</i> , <i>Carbon</i> , 2021, 182 , 144.
H ₂ SO ₄ /PVA gel	TpOMe-DAQ COF	Only as electrode material	84	0.25	A. Halder <i>et al.</i> , <i>J. Am. Chem. Soc.</i> , 2018, 140 , 10941.
3M KOH	Phos-COF-1	Only as electrode material	46	1	M. Sajjad <i>et al.</i> , <i>J. Energy Storage</i> , 2021, 44 , 103318.
1 M H ₂ SO ₄	FCTF	Only as electrode material	173	1	Y. Gao <i>et al.</i> , <i>Chem. Eng. J.</i> , 2020, 400 , 125967.

6 M KOH	N-doped C/g-C ₃ N ₄	Only as electrode material	129.3	1	M. Ibrahim <i>et al.</i> , ACS Appl. Energy Mater., 2022, 5, 12828
MG-Co-Li	MG-Co xerogel	Both as electrolyte and electrode material	86	1	This work

References

1. V. K. Pandey, M. K. Dixit, S. Manneville, C. Bucher and M. Dubey, *J. Mater. Chem. A*, 2017, **5**, 6211.
2. Y. Kumar and M. Dubey, *Chem. Commun.*, 2022, **58**, 549.